NASA TECHNICAL NOTE

NASA TN D-7126

NASA TN D-7126

DETERMINATION OF THE TEMPERATURE OF GAS MIXTURES BY USING LASER RAMAN SCATTERING

by Thom A. Coney and Jack A. Salzman

Lewis Research Center

Cleveland, Ohio 44135

NATIONAL AERONAUTICS AND SPACE ADMINISTRATION • WASHINGTON, D. C. • JANUARY 1973

DETERMINATION OF THE TEMPERATURE OF GAS MIXTURES BY USING LASER RAMAN SCATTERING

by Thom A. Coney and Jack A. Salzman

Lewis Research Center

SUMMARY

A theoretical model of the Raman rotational spectrum of a gas mixture was formulated and applied to an air mixture of oxygen and nitrogen. Theoretical spectra were calculated as a function of temperature and compared directly to spectra obtained experimentally. The comparison, made at temperatures within the range 243 to 313 K, showed the model to be accurate. An error analysis was then performed yielding theoretical and experimental temperature measurement accuracies. The theoretical error predicted for the temperature range used was ±20 K (~7 percent), which compared well with experimental data. The best experimental error was ±13 K (~5 percent). It was concluded that, within the limits of this experiment and the preceding accuracies, the temperature of a gas mixture can be measured by using Raman scattering.

INTRODUCTION

Laser systems have found many applications in the atmospheric sciences as tools for the remote measurement of meteorological variables. Some of the variables now being measured on an experimental basis include aerosol content, atmospheric density, atmospheric composition, and pollutant concentrations (refs. 1 to 3). Atmospheric temperature is a variable that at present is not being measured remotely by laser techniques.

Cooney suggested a method that might be used to implement this measurement (ref. 4). Because the intensity distribution of Raman-scattered light is a function of temperature, it is theoretically possible to measure the air temperature by analyzing its Raman spectrum. By using an optical radar (lidar) system such as is described in reference 5, two or more portions of the spectrum of a remote volume of air can be

measured simultaneously. The ratio of these measurements can then be related to the temperature of the volume of air. (Ratios of spectral intensities are used so that consideration need not be given to fluctuations in the index of refraction, water vapor, and particle concentrations, etc., in the intervening atmosphere.) The feasibility of using this method was demonstrated by Salzman, Masica, and Coney (ref. 6). In that study, it was shown that the temperature of a single gas system could be measured by analyzing Raman-scattered laser light. To relate the temperature of a volume of air to its Raman spectrum, it was necessary to expand that analysis so that application could be made to a mixture of gases.

This investigation was conducted to formulate a theoretical expression representing the Raman spectrum of air (and thus determine its temperature dependence) and to confirm the results by comparison with experimental data. This report presents a summary of this theoretical and experimental analysis. The primary consideration here is with the nitrogen-oxygen combination in air. Because the ratio of the cross sections for rotational Raman scattering of nitrogen and oxygen is an integral part of this analysis and because the available (theoretical) value appears to be too inaccurate, specific attention was given to its measurement. Experimental data are also presented showing the variation in the spectrum of air as a function of temperature for a temperature range of 243 to 313 K and a pressure of 1 atmosphere. The data were obtained on a Raman spectrophotometer.

ANALYSIS OF RAMAN SPECTRAL INTENSITY

When light is incident upon a molecular system, a quantum mechanical interaction takes place between a small portion of the light energy and the rotational states of the system. Raman scattering of the incident light can result. Because of the quantized nature of the rotational energy levels, the Raman-scattered light is shifted to the discrete wavenumbers $\nu_0 \pm \Delta\nu_j$, where ν_0 is the wavenumber of the incident light and $\Delta\nu_j$ is the wavenumber associated with the j^{th} quantized level, $\nu_0 - \Delta\nu_j$ represents an absorption of energy by the molecule (Stokes interaction), and $\nu_0 + \Delta\nu_j$ represents an emission of energy (anti-Stokes interaction). The rotational Raman spectrum is a measure of the intensity of the scattered light as a function of wavenumber. The molecular system of interest in this study is air; consequently, the Raman spectrum produced by a gas mixture must be analyzed.

The spectral intensity $I(\nu)$ of a mixture of independent gases is the sum of the spectral intensities of the component spectra corrected for the relative concentrations and Raman-scattering cross sections of the components:

$$I_{mixture}(\nu) = I_{comp\ 1}(\nu) + KI_{comp\ 2}(\nu) + K_1 I_{comp\ 3}(\nu) + \ldots \quad (1)$$

where K, K_1, etc., are correcting constants normalized to component 1. (All symbols are defined in appendix A.) Therefore, the theoretical Raman spectrum of air can be obtained by an independent analysis of the spectra produced by each constituent of air. Since nitrogen and oxygen make up approximately 99 percent by volume of the contents of air, the following analysis is limited to their contributions. Equation (1) thus becomes

$$I_{air}(\nu) = I_N(\nu) + KI_O(\nu) \tag{2}$$

with K related to the ratios of the concentrations and cross sections of oxygen and nitrogen.

A typical experimental Raman spectrum of a single gas system, in this case nitrogen, is shown in figure 1. Each line profile in such a spectrum of a single gas can be written in terms of a line shape function $S(\nu, \nu_j)/A_j$ normalized to a relative peak height I_j (A_j is a normalizing constant). It is shown in reference 6 that, for an analysis of a single-gas-system spectra, it is sufficient to consider only I_j (i.e., one can approximate the spectrum in fig. 1 by a line spectrum) and that, therefore, only peak heights need be measured in most experiments of this type. This approximation is not satisfactory for analyses of the oxygen-nitrogen system being considered herein because the line positions of the component spectra are different and partial or complete overlapping is likely. Since peak height is again generally the experimentally measured parameter, it is necessary to take into account contributions to each peak made by adjacent peaks. This can only be done by retaining in the theoretical analysis the line shape function $S(\nu, \nu_j)$. The spectral intensity of an isolated peak is therefore given by the equation

$$I_j(\nu) = \frac{I_j S(\nu, \nu_j)}{A_j} \tag{3}$$

where A_j normalizes the shape function to a peak value of 1, ν_j is the wavenumber of the center of the peak, and j is the quantum number associated with the energy level involved in the Raman interaction producing the peak. The normalized shape function, I_j, and ν_j are designated in figure 1 for the Stokes j-value of 12. The total spectrum of a single gas system is the sum of all the peaks resulting from each of the many possible rotational energy level transitions:

$$I(\nu) = \sum_j I_j \frac{S(\nu, \nu_j)}{A_j} \tag{4}$$

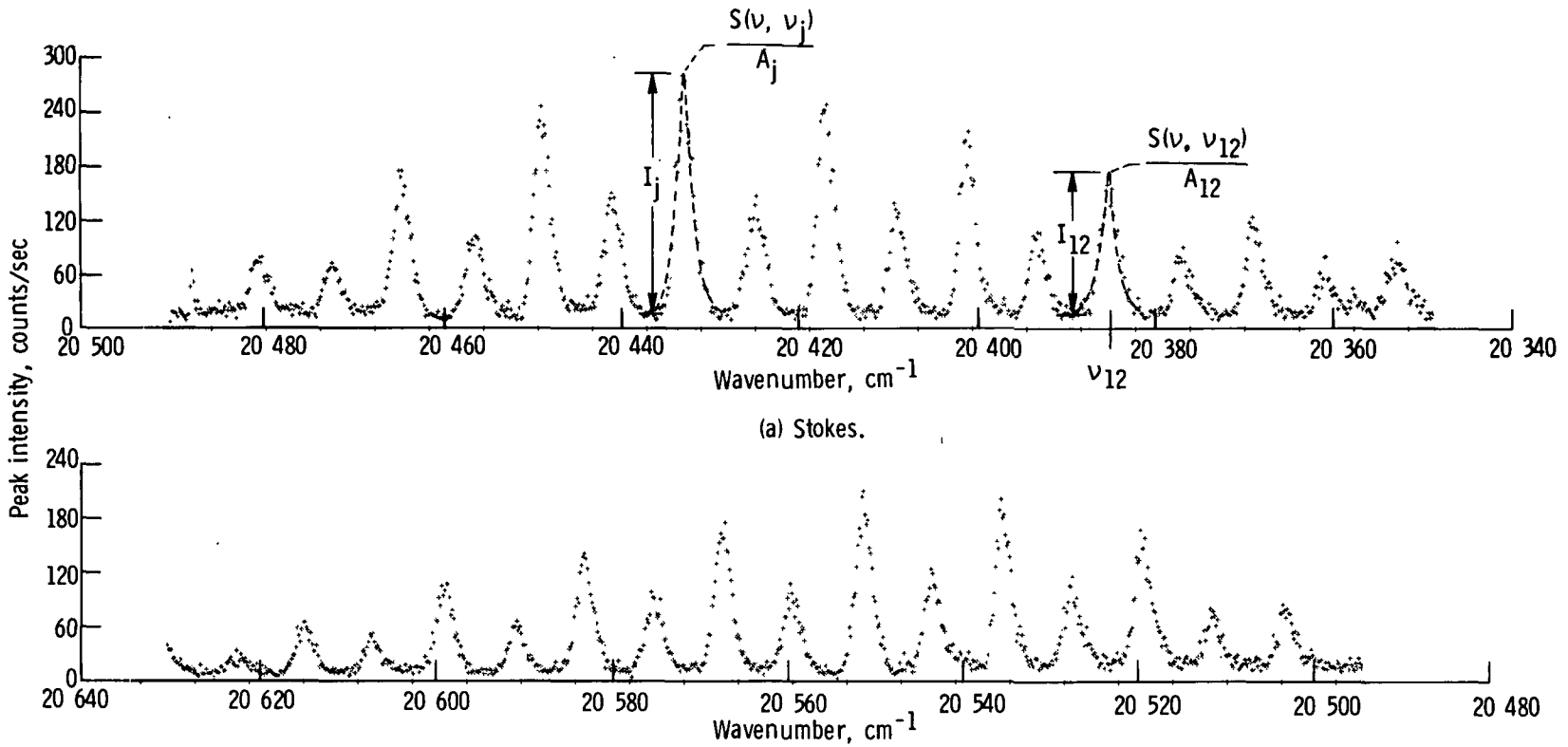

Figure 1. - Experimental spectrum of a single gas system - nitrogen. (Mie and Rayliegh scattered light, i.e., $\Delta\nu_j = 0$ is centered at 20 492 cm^{-1}.)

Substituting this equation into equation (2) yields the spectral intensity of air as a function of wavenumber:

$$I_{air}(\nu) = \sum_j I_j^N \frac{S^N(\nu, \nu_j)}{A_j^N} + K \sum_j I_j^O \frac{S^O(\nu, \nu_j)}{A_j^O} \tag{5}$$

Raman Line Intensity

An analysis of the relative peak intensities of an ideal line spectrum of a linear, diatomic molecule such as oxygen or nitrogen was performed in reference 6. Because these spectra result from molecular-energy-level transitions from the initial state j to j + 2 and j - 2, the line intensity I_j is determined by two component equations. It is shown in reference 6 that the line intensity of the Stokes half of the spectrum (j → j + 2) is

$$I_j^S = \frac{C(j+1)(j+2)}{2j+3} \frac{\theta}{T} \left(\nu_0 - \Delta\nu_j^S\right)^4 \exp\left[-j(j+1)\frac{\theta}{T}\right] \tag{6}$$

where

$$\Delta\nu_j^S = \frac{4k\theta}{hc}\left(j + \frac{3}{2}\right)$$

and of the anti-Stokes intensity (j → j - 2) is

$$I_j^{AS} = \frac{Cj(j-1)}{2j-1} \frac{\theta}{T} \left(\nu_0 + \Delta\nu_j^{AS}\right)^4 \exp\left[-j(j+1)\frac{\theta}{T}\right] \tag{7}$$

where

$$\Delta\nu_j^{AS} = \frac{4k\theta}{hc}\left(j - \frac{1}{2}\right)$$

The constant C in equations (6) and (7) is a proportionality constant which includes a nuclear spin degeneracy factor, θ is the rotational characteristic temperature of the

scattering gas, and T is the gas temperature.

It should be noted that O_2 has a ground-state spin and therefore has a more complicated intensity distribution than is given by equations (6) and (7). However, because the variations due to this spin are only significant at very low temperatures ($<<200$ K), they were considered negligible for the purposes of this study.

Equations (6) and (7) relate the spectral intensity of the ideal line spectrum of a single gas system to the gas temperature. The effect of this temperature dependence on the rotational envelope of the line spectrum of nitrogen is illustrated in figure 2. At the low temperature T_1, most of the nitrogen molecules populate the low energy levels and the line spectrum is "grouped" near the ground state (j = 0). As the temperature of the gas is increased (e.g., to T_3), more of the molecules populate the high energy states and the spectrum appears more evenly distributed.

The alternating intensity of the odd and even j-lines in figure 2 is a result of the nuclear spin degeneracy of nitrogen. Because of the spin degeneracy, the intensity of the odd j-lines is one-half the intensity of the even j-lines. In the case of oxygen, the spin degeneracy is such that the even j-lines have zero intensity.

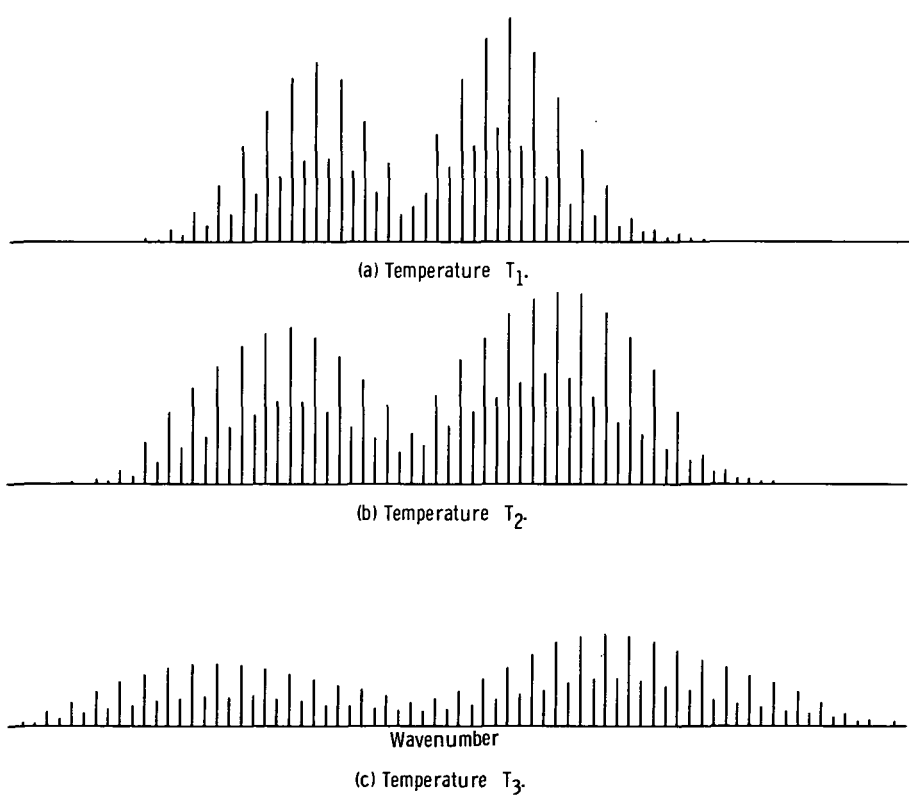

(a) Temperature T_1.

(b) Temperature T_2.

(c) Temperature T_3.

Figure 2. - Temperature variation of line spectrum of single gas system - nitrogen. $T_1 \ll T_2 \ll T_3$.

Equations (6) and (7) are related to the relative line intensity factor I_j used in equation (5) by the equation

$$I_j = \begin{cases} I_j^S & \text{for} \quad j \rightarrow j + 2 \quad \text{(Stokes)} \\ I_j^{AS} & \text{for} \quad j \rightarrow j - 2 \quad \text{(anti-Stokes)} \end{cases}$$

Rewriting equation (5) to reflect the distinction between portions of the Raman spectrum yields

$$I_{air}^S(\nu) = \sum_j I_j^{S,N} \frac{S^N\left(\nu, \nu_j^S\right)}{A_j^N} + K \sum_j I_j^{S,O} \frac{S^O\left(\nu, \nu_j^S\right)}{A_j^O} \tag{8}$$

$$\nu_j^S = \nu_0 - \Delta\nu_j^S \tag{8a}$$

$$I_{air}^{AS}(\nu) = \sum_j I_j^{AS,N} \frac{S^N\left(\nu, \nu_j^{AS}\right)}{A_j^N} + K \sum_j I_j^{AS,O} \frac{S^O\left(\nu, \nu_j^{AS}\right)}{A_j^O} \tag{9}$$

$$\nu_j^{AS} = \nu_0 + \Delta\nu_j^{AS} \tag{9a}$$

Note that $I_j^S = I_j^S(\theta_N)$, etc.

The same shape function is used for both sides of the spectrum since the same molecular levels are involved in the transitions producing the two sides. The difference is only in the direction of the transition; that is, the Stokes side results from an absorption of energy by the molecule while the anti-Stokes side results from an emission of energy.

Spectral Line Broadening

An evaluation of the shape function involves an analysis of the effects of line broadening and instrument distortion on an ideal line spectrum such as that shown in figure 2.

Attention is first given to the profiles resulting from Doppler broadening, natural line broadening, and pressure broadening and to the profile resulting from their interaction. Instrument distortion is included in the analysis by applying the appropriate monochromator slit function to the resultant profile. Another factor classified as instrument distortion is contributed by the detection and recording electronics. A theoretical analysis of this factor was not made. Rather it was assumed that bandwidth only would be affected and that the magnitude of this effect could be determined experimentally.

It was expected that for this study the slit function would be the dominant factor in establishing the shape and bandwidth of the final theoretical spectrum. However, the other broadening factors were included in the analysis to determine the magnitude of their effect and to ensure completeness.

Doppler broadening. - For this study the incident light energy is that produced by a continuous-wave, gas laser. Because the laser emission source is a gas of highly mobile ions, the output of the laser is Doppler broadened. The distribution resulting from this broadening is Gaussian in wavenumber (ref. 7) as given by

$$S_{laser}(\nu) = \exp\left[-\frac{2.77}{R_L^2}(\nu - \nu_0)^2\right] \tag{10}$$

where R_L is the half-width of the laser emission and ν_0 is the center emission line. When applied to the calculation of the Raman line shape, ν_0 becomes ν_j.

Natural line broadening. - The energy levels of the target molecules represent a second source of line broadening. This broadening takes several forms, included among which are natural line broadening and those forms collectively referred to as pressure broadening (e.g., collision, Stark, and impact broadening). The first, natural line broadening, results because of the uncertainty associated with the value of the emission wavenumber ν of a molecule radiating from an upper level to a lower level (ref. 8). By evaluating the probability distribution of the energy of the upper and lower levels, a distribution as a function of wavenumber is obtained

$$S_{nat}(\nu) = \frac{\frac{1}{2c\pi}\left(\frac{1}{\tau_j} + \frac{1}{\tau_{j+2}}\right)}{(\nu - \nu_j)^2 + \frac{1}{4c^2\pi^2}\left(\frac{1}{\tau_j} + \frac{1}{\tau_{j+2}}\right)^2} \tag{11}$$

where τ_j and τ_{j+2} are the lifetimes of the j^{th} and $(j + 2)^{th}$ levels. The bandwidth of natural broadening calculated from the Lorentz-type distribution is

$$\frac{1}{\pi c}\left(\frac{1}{\tau_j} + \frac{1}{\tau_{j+2}}\right)$$

which corresponds to the uncertainty in ν_j as dictated by the Heisenberg uncertainty principle.

Pressure broadening. - The second type of broadening, pressure broadening, mentioned in the preceding section refers to those mechanisms whose effect increases with pressure. As with natural broadening, these generally produce Lorentz-type distributions

$$S_{press}(\nu) = \frac{R_P/2}{(\nu - \nu_j)^2 + \left(\frac{R_P}{2}\right)^2} \tag{12}$$

where R_P is the bandwidth due to pressure broadening. The combined effect of natural and pressure broadening is simply

$$S_{Raman}(\nu) = \frac{R_R/2}{(\nu - \nu_j)^2 + \left(\frac{R_R}{2}\right)^2} \tag{13}$$

where

$$R_R = \frac{1}{\pi c}\left(\frac{1}{\tau_j} + \frac{1}{\tau_{j+2}}\right) + R_P$$

and is the bandwidth due to natural and pressure broadening (ref. 8).

The Raman-scattered light emitted by the molecules is the result of the interaction between the Doppler-broadened incident light energy and the natural- and pressure-broadened molecular energy levels. The resulting distribution about an emission wavenumber ν_j is given by the relation

$$S_{Voigt}(\nu, \nu_j) = \int_{-\infty}^{\infty} S_{laser}(\nu') S_{Raman}(\nu, \nu', \nu_j) d\nu' \tag{14}$$

or

$$S_{Voigt}(\nu, \nu_j) = \int_{-\infty}^{\infty} \frac{\exp\left[-\frac{2.77}{R_L^2}(\nu' - \nu_j)^2\right]}{(\nu' - \nu)^2 + \left(\frac{R_R}{2}\right)^2} d\nu' \qquad (15)$$

where ν' is a dummy variable of integration.

Equation (15) is commonly referred to as the Voigt function (ref. 8) and represents the broadened Raman spectral output for the j^{th} rotational level transition. Since a closed-form solution to this equation is not available, the emission line profile was obtained numerically. Figure 3 shows the theoretical profile resulting from the interaction of incident light having a line width of 0.166 cm^{-1} with a Raman energy level having a line width of 0.075 cm^{-1}. As is indicated in the figure, the bandwidth of the resulting emission profile is 0.212 cm^{-1}.

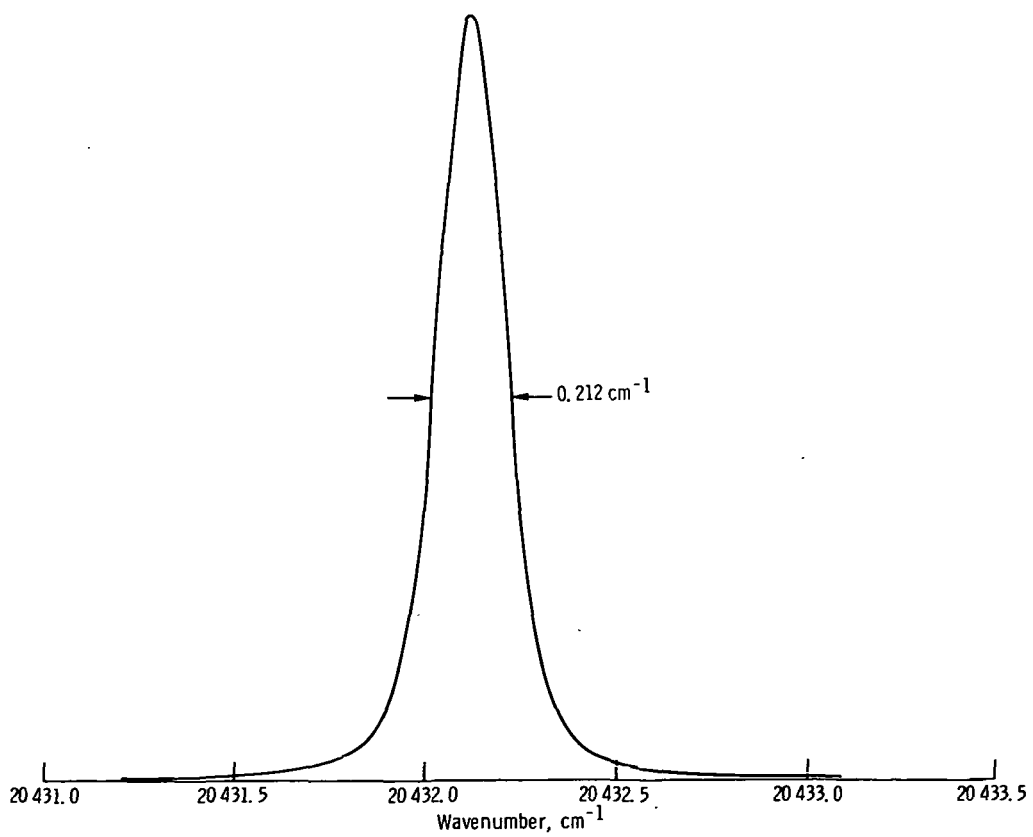

Figure 3. - Numerical solution to Voigt function using 0.166 cm^{-1} for laser line width and 0.075 cm^{-1} for Raman line width.

Instrument distortion. - The instrumentation used to measure spectral intensity as a function of wavenumber was a single-pass monochromator used in conjunction with photon-counting detection electronics. (This equipment is discussed in appendix B.) Most instrument distortion of the spectral line shapes is produced by the monochromator as a result of "nonlinear transmission characteristics" of the slits (ref. 9). Because of the finite width of the entrance and exit slits and because of the imperfect resolution of the grating, a band of wavenumbers is transmitted. The distribution as a function of wavenumber of this transmitted light is commonly referred to as the slit function $S_s(\nu)$.

Because the slit function has a major effect on the shape and bandwidth of the measured spectrum, its incorporation into the theoretical calculations is essential. An evaluation of the transmission characteristics of the monochromator used in this study suggested that either of the two commonly used slit functions (refs. 9 to 11) might be applicable. The two functions are the triangular slit function, having a half-width equal to the geometric slit width R_s of the monochromator, and the Gaussian function

$$S_s(\nu) = \exp\left[-\frac{2.77}{R_s^2}(\nu - \nu_s)^2\right] \tag{16}$$

where ν_s is the wavenumber setting on the monochromator. Both of these functions were used analytically to determine which best reproduced an experimental Raman line profile. For the spectral system under study here, the Gaussian slit function was found to be the better approximation. Consequently, this function was used in all further analysis.

The interaction of a slit function with a line-broadened emission profile is illustrated in figure 4. The Raman emission line profile $S_{Voigt}(\nu, \nu_j)$ is centered at ν_j and the slits are centered at ν_s. The intensity of the light transmitted by the slits is proportional to the area (shaded in fig. 4) under the emission profile adjusted by the slit function. Written in general, by letting $\nu_s \rightarrow \nu$, this is

$$S(\nu, \nu_j) = \int_{-\infty}^{\infty} S_s(\nu, \nu')S_{Voigt}(\nu', \nu_j)d\nu'$$

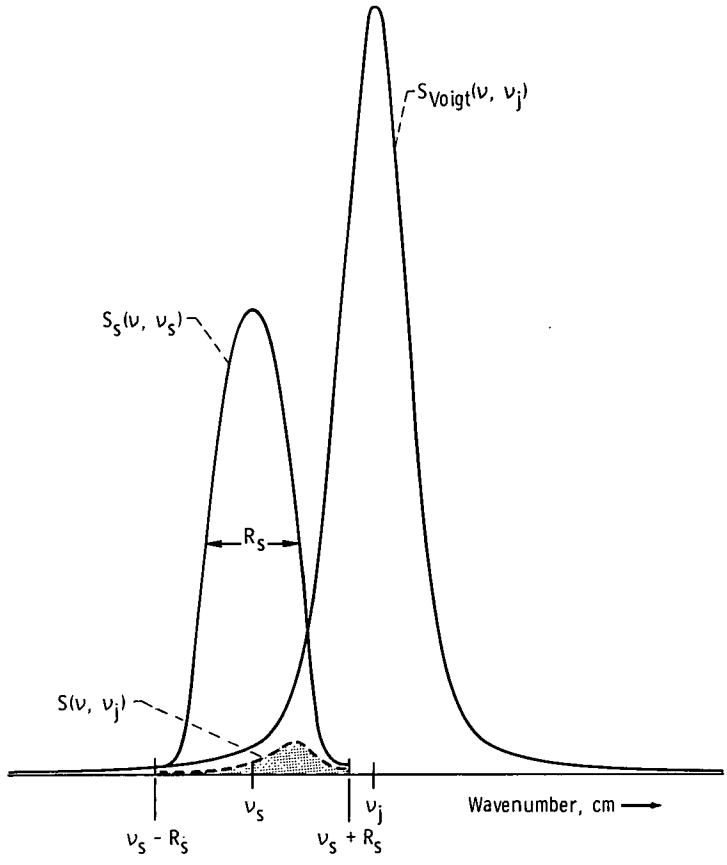

Figure 4. - Interaction between slit function and Voigt function.

Substituting equations (15) and (16) into this equation yields

$$S(\nu, \nu_j) = \int_{-\infty}^{+\infty} \exp\left[-\frac{2.77}{R_s^2}(\nu' - \nu)^2\right] \int_{-\infty}^{\infty} \frac{\exp\left[-\frac{2.77}{R_L^2}(\nu'' - \nu_j)^2\right]}{(\nu'' - \nu')^2 + \left(\frac{R_R}{2}\right)^2} d\nu'' \, d\nu' \tag{17}$$

The normalizing constant A_j is obtained by setting $\nu = \nu_j$,

$$A_j = S(\nu_j, \nu_j) \tag{17a}$$

Figure 5 shows the solution of equation (17) for $R_L = 0.166$ cm^{-1}, $R_R = 0.075$ cm^{-1}, and a slit width of 1.84 cm^{-1}. Again, the solution was obtained numerically. The band-

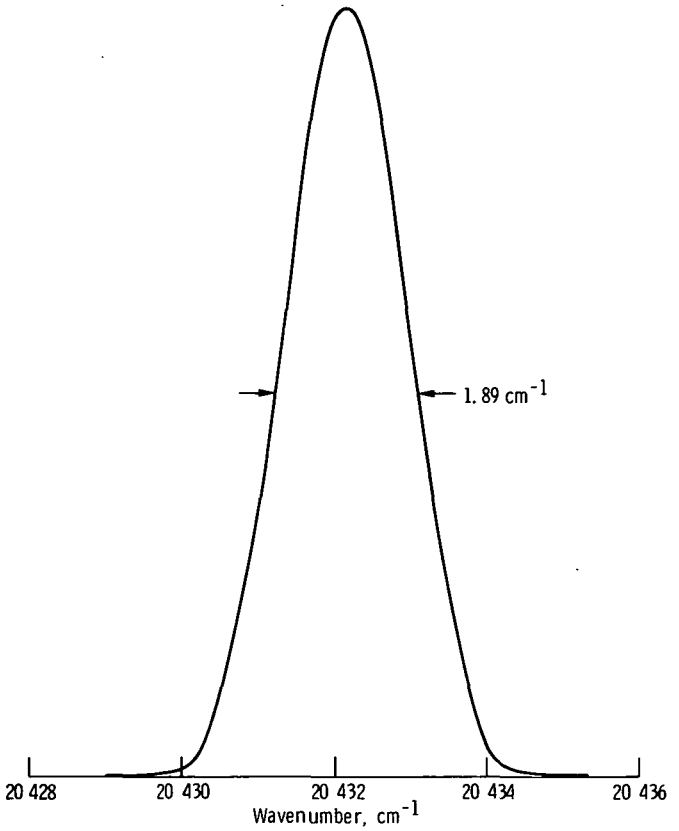

Figure 5. - Line profile resulting from combination of slit function and Voigt profile for slit width of 1.84 cm^{-1}. Laser line width, 0.166 cm^{-1}; Raman line width, 0.075 cm^{-1}.

width of the resultant profile is 1.89 cm^{-1}.

Interference filter transmission. - In the case where interference filters are used in place of a monochromator, the shape function is equal to the Voigt function. Therefore, equation (5) becomes

$$I_{air}(\nu) = \sum_j I_j^N \frac{S_{Voigt}^N(\nu, \nu_j)}{A_j^N} + K \sum_j I_j^O \frac{S_{Voigt}(\nu, \nu_j)}{A_j^O}$$

$$A_j = S_{Voigt}(\nu_j, \nu_j)$$

The total transmission of a filter is

$$I_{total} = \int_{-\infty}^{\infty} S_F(\nu) I_{air}(\nu) d\nu$$

The transmission of the filter is thus related to the temperature of the scattering gas through the relative peak intensities I_j^N and I_j^O contained in I_{air}.

Calculation of a Theoretical Raman Spectrum

Incorporating the results from the preceding analysis of line intensity and line shape into equations (8) and (9) yields a set of equations for the theoretical Raman rotational spectrum of air. These equations are presented in table I. The equations in this table are referred to by Roman numerals.

TABLE I. - EQUATIONS FOR THEORETICAL RAMAN ROTATIONAL SPECTRUM OF AIR

I	$I_{air}^S(\nu) = \sum_j I_j^{S,N} \frac{S^N(\nu, \nu_j^S)}{A_j^N} + K \sum_j I_j^{S,O} \frac{S^O(\nu, \nu_j^S)}{A_j^O}$ $I_{air}^{AS}(\nu) = \sum_j I_j^{AS,N} \frac{S^N(\nu, \nu_j^{AS})}{A_j^N} + K \sum_j I_j^{AS,O} \frac{S^O(\nu, \nu_j^{AS})}{A_j^O}$
II	$I_j^S = C \frac{(j+1)(j+2)}{2j+3} \frac{\theta}{T} \left(\nu_j^S\right)^4 \exp\left[-j(j+1)\frac{\theta}{T}\right]$ $I_j^{AS} = C \frac{j(j-1)}{2j-1} \frac{\theta}{T} \left(\nu_j^{AS}\right)^4 \exp\left[-j(j+1)\frac{\theta}{T}\right]$
III	$S(\nu, \nu_j) = \int_{-\infty}^{\infty} \exp\left[-\frac{2.77}{R_s^2}(\nu' - \nu)^2\right] \int_{-\infty}^{\infty} \frac{\exp\left[-\frac{2.77}{R_L^2}(\nu'' - \nu_j)^2\right]}{(\nu'' - \nu')^2 + \left(\frac{R_R}{2}\right)^2} d\nu'' \, d\nu'$
IV	$A_j = S(\nu_j, \nu_j)$
V	$I_j^{S,N} = I_j^S(\theta_N)$
VI	$\nu_j^S = \nu_0 - \Delta\nu_j^S(\theta)$ $\nu_j^{AS} = \nu_0 + \Delta\nu_j^{AS}(\theta)$

Calculating a theoretical spectrum of air by using these equations involved the determination and substitution of all pertinent constants, that is, the rotational characteristic temperatures θ_N and θ_O and the appropriate bandwidths, and included a comparison of the component equations (II) to (VI) with experimental data.

Rotational characteristic temperature. - The generally accepted values for the rotational characteristic temperatures of nitrogen and oxygen are 2.862 K (ref. 12) and 2.082 K (ref. 13), respectively. The value given for θ_N was shown in reference 6 to reproduce accurately the line positions of an experimental spectrum of nitrogen. However, a similar comparison between predicted and experimental line positions for oxygen made in the study reported herein showed considerable misalinement. (The experimental procedure and apparatus used is discussed in appendix B.) These data indicated that θ_O equaled 2.06 K. This value also agreed very well with data presented by Stoicheff (ref. 12). By using those data, a value of 2.065 K was calculated. This latter value was used in all further calculations of the air spectrum.

Bandwidths. - The constants to be substituted into the shape function include the slit width R_S, the bandwidth of the laser R_L, and the bandwidth of the Raman energy level R_R. The value substituted for R_S is simply the slit-width setting on the monochromator used to obtain the experimental spectrum. A value of 0.166 cm^{-1} for R_L was supplied in the manufacturer's data for the laser.

The bandwidth of the Raman energy level R_R was evaluated through a review of references 14 and 15. Reference 14 provided a discussion of the bandwidth as a function of the quantum number j, and reference 15 listed R_R as a function of the gas species. Experimental data presented in reference 14 showed a variation in R_R with j such that $R_R(j=7) = 0.08 \pm 0.01$ and $R_R(j=12) = 0.061 \pm 0.01$ cm^{-1}. To determine the significance of this variation on the Raman emission profile and on the spectrum profile, equations (15) and (17) were evaluated for R_R of 0.085 cm^{-1} and 0.065 cm^{-1}. Values used for R_L and R_S were 0.166 cm^{-1} and 1.84 cm^{-1}, respectively. For this change in R_R of 0.02 cm^{-1}, the bandwidth of $S_{Voigt}(\nu, \nu_j)$ changed approximately 6 percent and the bandwidth of $S(\nu, \nu_j)$ changed approximately 1 percent. This variation was considered negligible for this study and it was assumed that R_R was a constant equal to 0.075 cm^{-1}. Because reference 15 indicated that the bandwidths of oxygen and nitrogen were the same, R_R^O was also set equal to 0.075 cm^{-1}.

With the inclusion of these values for R_S, R_L, and R_R into equations (I) with K = 0, a theoretical line profile for a single gas system of nitrogen was calculated. A comparison was then possible between the theoretical and experimental bandwidths and line shapes. The experimental bandwidth exceeded the theoretical by about 8 percent. This discrepancy was attributed to an additional distortion introduced by the response characteristics of the detection and recording electronics. The value of the slit width R_S used in the calculations was adjusted to account for this added distortion. This adjustment was made by first plotting the theoretical bandwidth as a function of R_S, as in

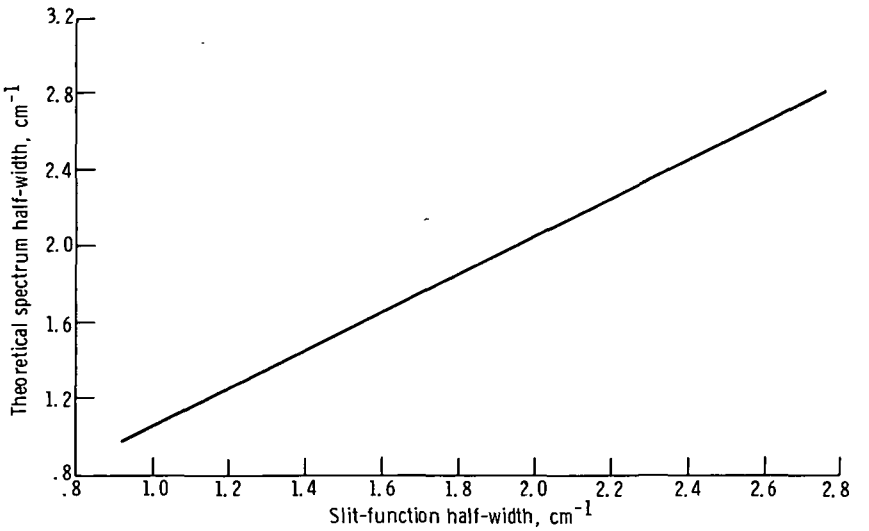

Figure 6. - Line width of theoretical spectrum as function of slit-function half-width for laser line width of 0.166 cm^{-1} and Raman line width of 0.075 cm^{-1}.

figure 6. This plot was then used by measuring the bandwidth of the experimental spectrum, locating this value on the abscissa, and using the corresponding value for R_s (ordinate) in equations (I).

With the inclusion of the broadening effects produced by the electronics, the theoretical spectrum of nitrogen reproduces very well the experimental spectrum. Figure 7 shows a comparison of a theoretical Raman spectrum of nitrogen with an experimental spectrum. The theoretical spectrum was calculated by using equations (I) with $K = 0$, and the constants and correction factor previously discussed. Peak heights were normalized according to the method described in appendix B. To proceed with the calculation of a Raman spectrum of air then required only an evaluation of the constant K.

Relative cross section. - As stated previously, the constant K is related to the Raman rotational cross sections σ of nitrogen and oxygen and to the molecular concentrations in air ρ of the two components. K is given by the equation

$$K = \frac{\rho_O \sigma_O}{\rho_N \sigma_N} \tag{18}$$

The percent concentrations of nitrogen and oxygen in air are well documented. Values obtained from reference 16 yield a molecular concentration ratio ρ_O/ρ_N of 0.27 at 1 atmosphere. Apparently, no experimental data presently exist concerning the rotational cross sections of nitrogen and oxygen. The only analytical values found were those presented by Melfi (ref. 1). They are $\sigma_N = 3.2 \times 10^{-29}$ cm^2 sr^{-1} and

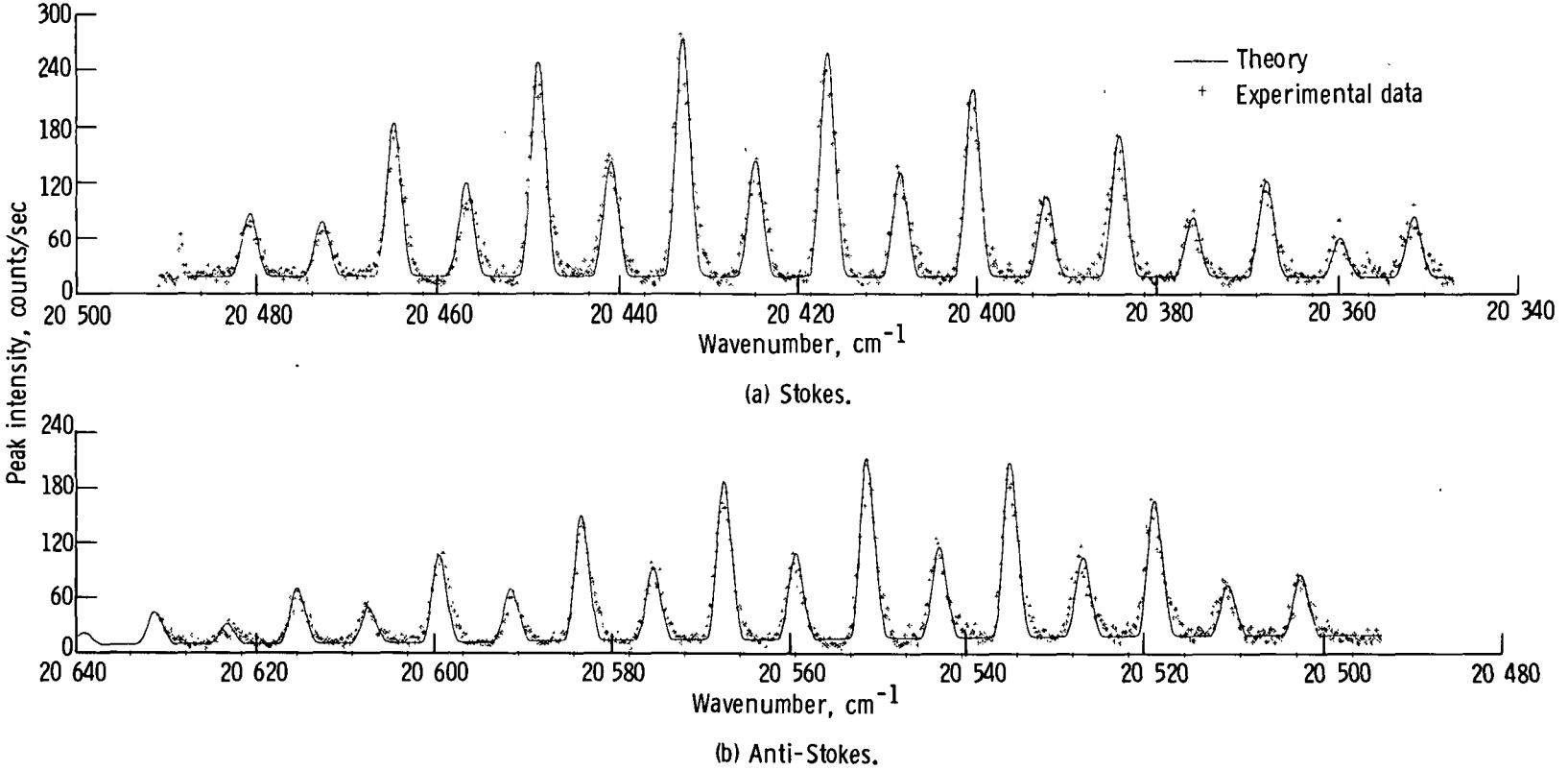

Figure 7. - Comparison of theoretical and experimental rotational spectra of nitrogen.

$\sigma_O = 5.1 \times 10^{-29}$ cm^2 sr^{-1}. Substituting these concentrations and cross sections into equation (19) resulted in a K-value of 0.43.

By using this value of K, a theoretical spectrum of air was calculated. A comparison was then made between the ratios of the oxygen to nitrogen peak heights measured from this spectrum and those measured from an experimental spectrum. Because these ratios did not agree, it was concluded that the accuracy of the theoretical value given for σ_O/σ_N (1.59) was inadequate. Consequently, data were obtained for the purpose of experimentally evaluating the relative cross sections of oxygen and nitrogen.

RESULTS AND DISCUSSION

Measurement of Relative Cross Section

The relative cross section of oxygen and nitrogen was measured by comparing theoretical rotational Raman spectra of air to experimental spectra and determining that value of K which resulted in the best agreement. For this purpose, experimental spectra were obtained (by using the apparatus and procedures described in appendix B) for monochromator slit-width settings of 0.92, 1.84, and 2.76 cm^{-1}. Peak intensities of each of these spectra were measured and documented and equations (I) were appropriately normalized.

Theoretical spectra were then calculated for various values of K at each slit-width setting. Since the relative molecular concentration of oxygen and nitrogen was assumed constant and fixed at 0.27, this variation in K resulted directly in a variation of the relative cross section σ_O/σ_N. Theoretical spectra were calculated for σ_O/σ_N values of 1.7, 2.0, and 2.3 at slit-width settings of 0.92 and 1.84 cm^{-1} and σ_O/σ_N values of 1.7, 2.15, and 2.6 at a setting of 2.76 cm^{-1}. The theoretical intensity of each of the oxygen lines was then measured and plotted as a function of σ_O/σ_N. Figure 8 is typical of the resulting graphs. Shown are the variations obtained by using a slit width of 1.84 cm^{-1}. (A line designation of O_3 refers to the resolved j=3 oxygen line while a designation of O_5-N_3 refers to the line resulting from some degree of irresolution between the j=5 oxygen and j=3 nitrogen lines.)

By using these graphs the relative cross sections corresponding to each of the experimental line intensities of oxygen were determined. An average was then calculated for each slit-width setting. Table II lists the lines used and the relative cross sections measured for the slit-width setting of 1.84 cm^{-1}. Average values obtained for settings of 0.92, 1.84, and 2.76 cm^{-1} are 2.11±0.38, 2.16±0.35, and 2.41±0.27, respectively. The apparent discrepancy in these values is not attributable to a poor fit between theoretical and experiment spectra, since in all cases they compared very well. However,

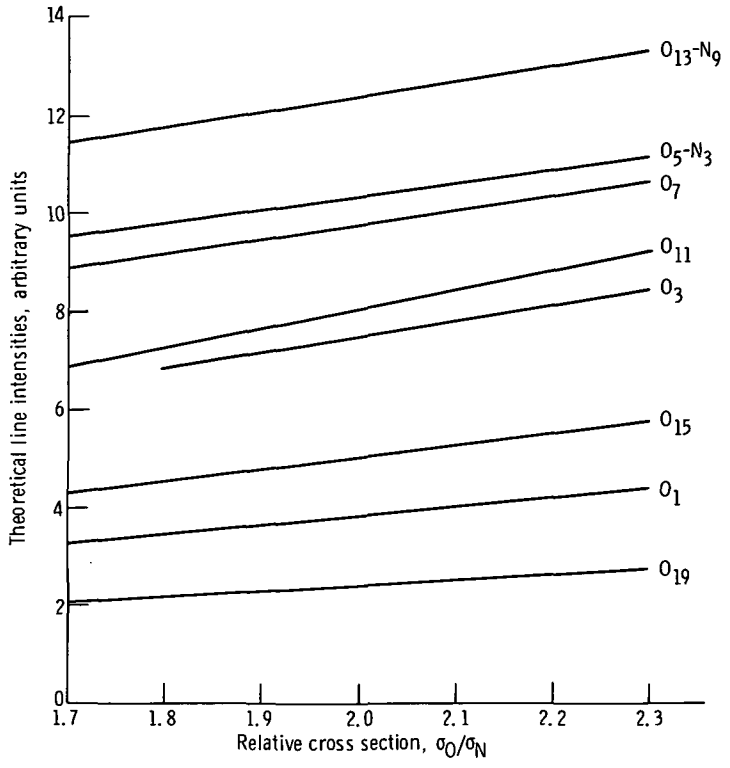

Figure 8. - Theoretical Stokes line intensity as function of relative cross section for slit width of 1.84 cm^{-1}.

TABLE II. - OXYGEN EXPERIMENTAL LINE INTENSITY AND CORRESPONDING RELATIVE CROSS SECTION FOR SLIT WIDTH OF 1.84 cm^{-1}

Stokes			Anti-Stokes		
Line	Intensity, counts/sec	Relative cross section	Line	Intensity, counts/sec	Relative cross section
O_1	33	1.45	O_3	37	1.70
O_3	96	2.18	O_5	85	2.17
O_5-N_3	129	2.24	O_7-N_5	110	2.23
O_7	121	2.21	O_9	95	1.85
O_9-N_6	253	2.02	O_{11}-N_8	208	2.37
O_{11}	106	2.22	O_{13}	83	2.38
O_{13}-N_9	138	1.78	O_{15}-N_{11}	104	2.09
O_{15}	61	2.04	O_{17}	55	2.75
O_{19}	33	2.30	O_{21}	23	2.68
O_{21}	18	1.75	O_{23}	15	2.81

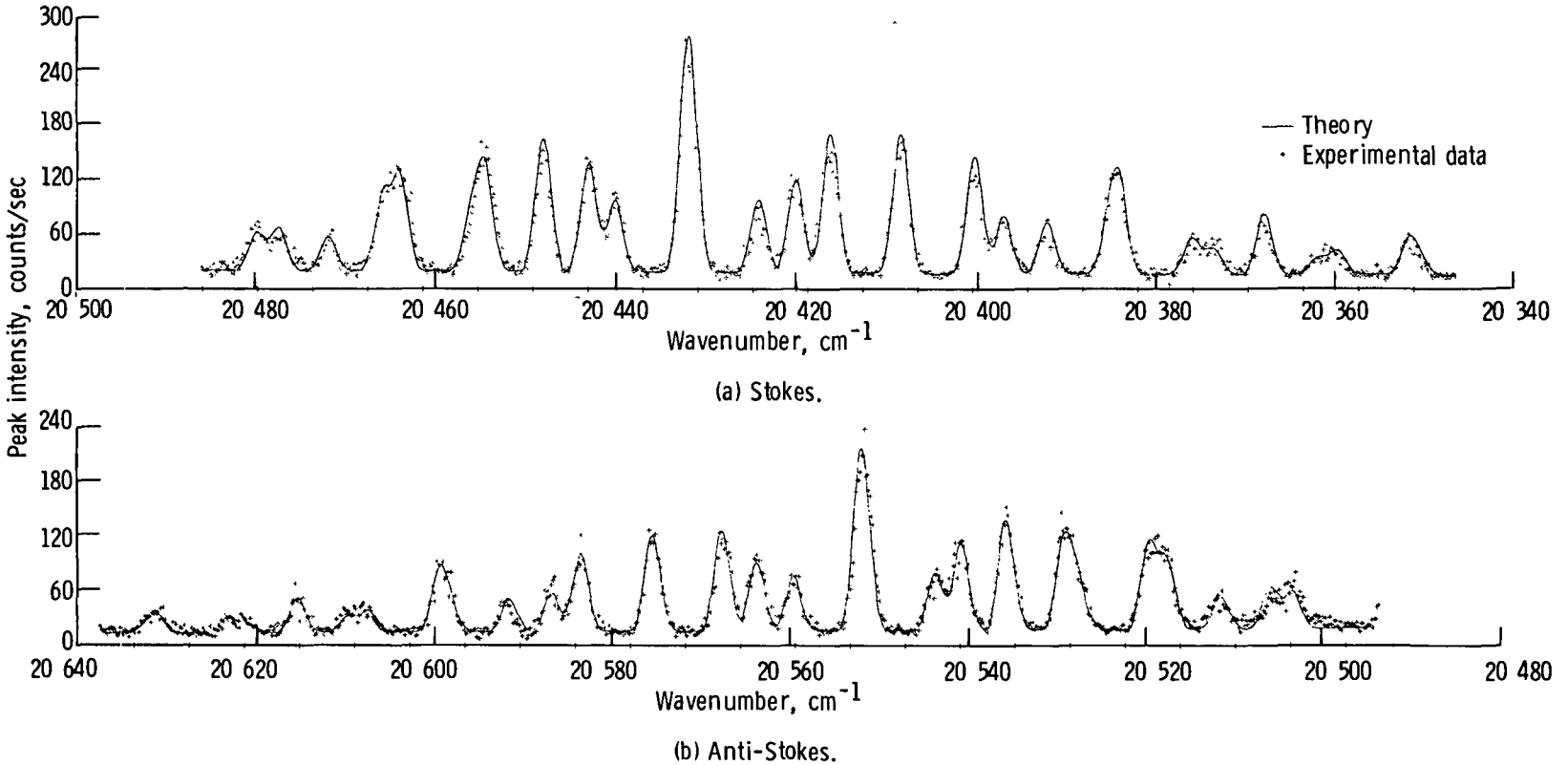

Figure 9. - Comparison of theoretical and experimental spectra of air.

the poor resolution resulting from a slit-width setting of 2.76 cm^{-1} limited the number of resolved oxygen lines and made base line and background intensities difficult to establish. Consequently, confidence was placed in the results obtained from the better resolved data, that is, those obtained using slit widths of 0.92 and 1.84 cm^{-1}. Taking the average of these two values resulted in a relative cross section of 2.14±0.36. Figure 9 shows a comparison between the theoretical spectrum calculated using this value and an experimental spectrum. In this case the slit width was 1.84 cm^{-1}.

Measurement of Air Temperature

The relations yielding the theoretical Raman rotational spectra of air are functions of the air temperature through the line intensity factors I_j^S and I_j^{AS}. The measurement of the gas temperature is accomplished by relating its temperature to the ratio of line intensities. Line ratios are used to eliminate extraneous effects such as encountered in the transmitting medium. This is especially important when considering a remote sensing system.

Because of the complexity of equations (I), it is not possible to obtain directly a solution for temperature in terms of the line ratios. Consequently, the solution was obtained graphically. First, to reduce the number of possible line ratios to be considered to a manageable quantity, an error analysis was performed. Reference 6 showed that the standard deviation of the temperature was given by the equation

$$\Delta T = \frac{1}{\text{Slope}} \left[\frac{I_{j_1}}{I_{j_2}} \left(\frac{I_{j_1} + I_{j_2}}{I_{j_2}^2} \right) \right]^{1/2} \tag{19}$$

where the slope is simply

$$\text{Slope} = \frac{\dfrac{I_{j_1}(T_1)}{I_{j_2}(T_1)} - \dfrac{I_{j_1}(T_2)}{I_{j_2}(T_2)}}{T_1 - T_2}$$

Therefore, theoretical spectra were calculated and all line intensities were measured for temperatures of 243 and 313 K. These are plotted in figure 10. To simplify notation, each peak in the spectra was assigned a number. The numbering started at the Rayleigh line and progressed arithmetically for each peak. For example, the O_7 Stokes line became the S6 line, and the N_7 anti-Stokes line became AS9. This numbering system

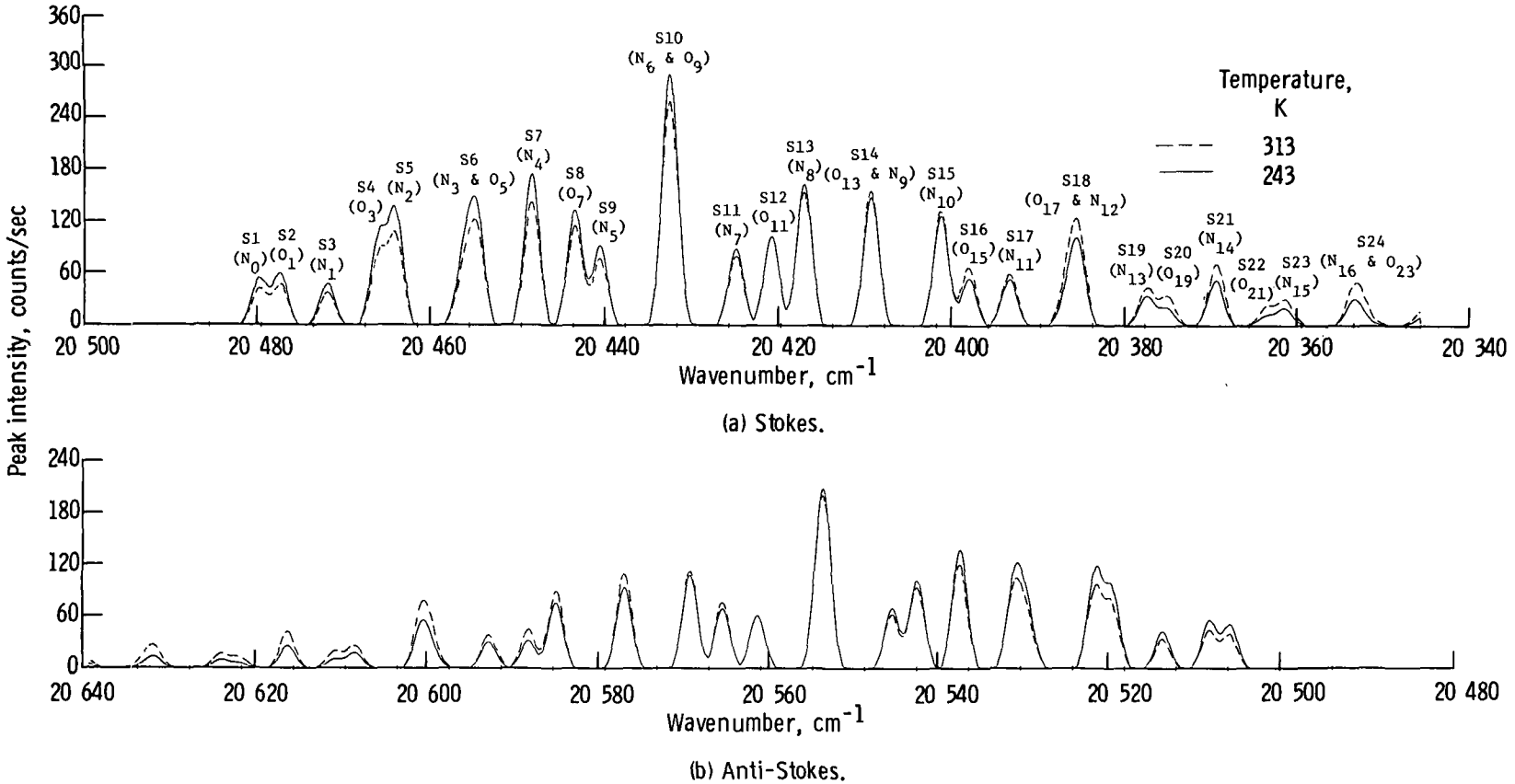

Figure 10. - Comparison of theoretical spectrum of air for temperatures of 243 and 313 K.

is illustrated in figure 10. By using equation (19) the standard deviation of the temperature for theoretical peak intensities normalized to typical experimental values was calculated for all line-ratio combinations. This included Stokes-to-Stokes, anti-Stokes-to-anti-Stokes, and anti-Stokes-to-Stokes ratios. The best standard deviation predicted was ±20 K. To determine the validity of equation (19), the standard deviation for each of these ratios was then compared to the standard deviations calculated from experimental data. To reduce the quantity of experimental data analyzed, attention was given only to those ratios which resulted in a theoretical ΔT of less than 25 K. Fifty-six line-ratio combinations satisfied this restriction. Because equation (19) is a conservative estimate of ΔT (ref. 6), it was expected that the experimental ΔT would be less than predicted.

Eight experimental spectra were obtained for comparison, two at each of the temperatures 243, 273, 299, and 313 K. The line intensities were then measured and appropriate ratio combinations calculated. Graphs were made showing the theoretical variation in these ratios as a function of temperature. Figure 11 presents a sampling

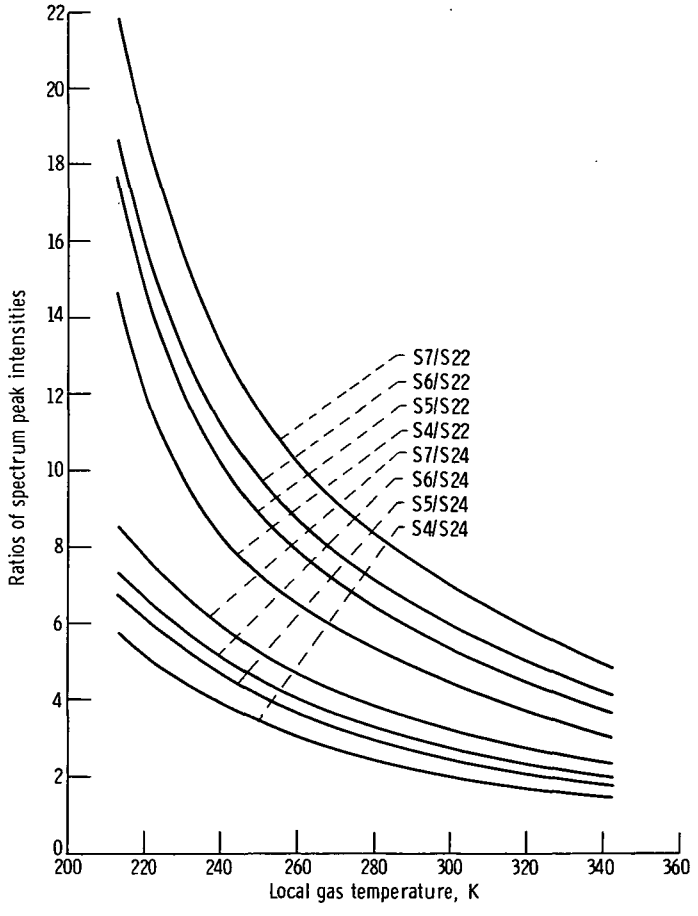

Figure 11. - Theoretical variation with temperature of ratios of Stokes lines 4 through 7 to Stokes lines 22 and 24.

of the resulting curves. The temperature corresponding to each experimental line ratio was determined by using these graphs, and experimental standard deviations were calculated. These deviations compared satisfactorily with those predicted from equation (19). The ratios best used to measure the temperature of the scattering gas were chosen on the basis of the experimental standard deviations. Considering those ratios with the lowest deviations wherein any single line intensity is used only once resulted in the selection of the following ratios: S7/S24, AS5/AS18, and AS24/S4. The temperatures obtained by using these ratios are compared to the actual air temperature in figure 12. It is concluded that a measurement of the air temperature is feasible within the temperature range and predicted accuracy of ±20 K presented here. Through the use of the selected lines an experimental accuracy of ±13 K was obtained. Since the accuracy of this measurement is strongly dependent on statistics, it is assumed that increased spectral intensity, the use of the ratios of multiple lines, or the use of the ratios of spectral bands such as obtained with interference filters would improve that accuracy.

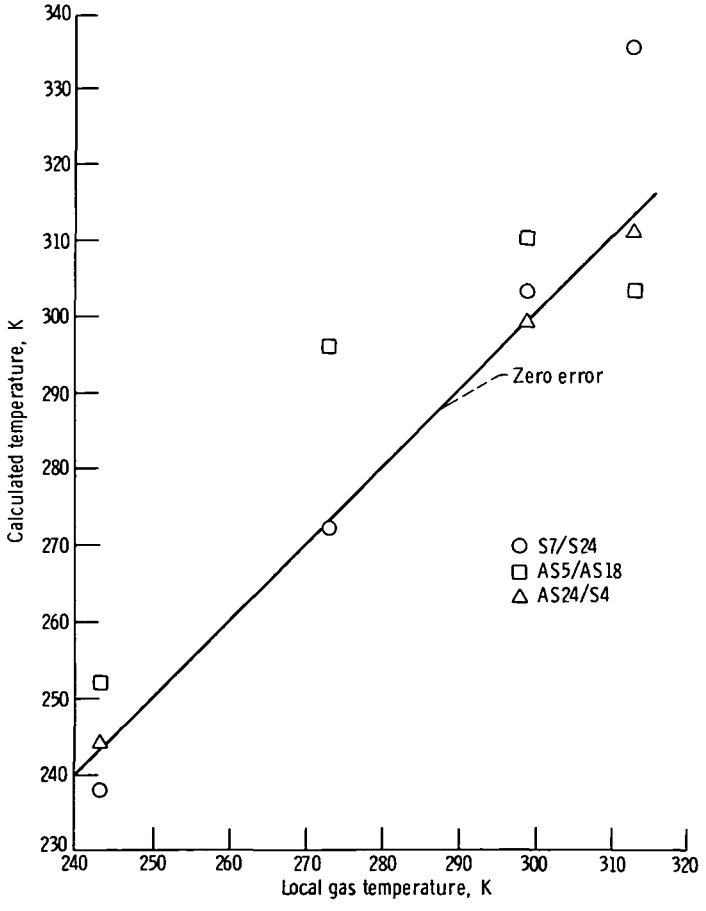

Figure 12. - Temperature measurement results calculated from the Stokes line ratio S7/S24, the anti-Stokes line ratio AS5/AS18, and the anti-Stokes/Stokes line ratio AS24/S4.

SUMMARY OF RESULTS

The purpose of the study reported herein was to formulate a theoretical expression that represented the Raman rotational spectrum of air and to confirm the results by comparison with experimental data. Specific attention was given to the dependence of this spectrum on temperature. First, an expression representing the spectrum of a single gas system (nitrogen) was formulated and verified by comparing a theoretical spectrum to a rotational spectrum obtained experimentally. Then considering only the major components of air (nitrogen and oxygen), their concentrations, their molecular properties, and the ratio of their Raman cross sections, two single gas spectra were combined to produce one theoretical spectrum of air. Again, experimental data and theory were compared with good agreement. The following specific results were obtained:

1. The measured Raman rotational spectrum of air results from the interaction of the Doppler-broadened laser output, the pressure-broadened Raman energy levels, and instrument distortion introduced by the monochromator and the detection and recording electronics. Table I presents the theoretical equations for the spectral intensity as a function of wavenumber.

2. The ratio of the rotational Raman cross section of oxygen to nitrogen is 2.14 ± 0.36.

3. The Raman rotational spectrum can be used to measure the temperature of air. The data obtained in this experiment yielded temperature measurement accuracies in agreement with those predicted for a single ratio by the statistics of the process, that is, approximately ±20 K. The use of selected experimental lines resulted in an experimental accuracy of ±13 K. By considering the average of several ratios and by increasing the statistics of the data, it is theoretically possible to improve this accuracy. Further improvement may be possible by considering the ratio of spectral bands such as are obtained by using interference filters rather than a monochromator. Because the basic theoretical spectrum is now available, it is a simple matter to superimpose upon it the transmission curves of a filter system and thus calculate the ratios of the transmission of those filters as a function of temperature as well as calculate temperature measurement accuracies.

Lewis Research Center,
National Aeronautics and Space Administration,
Cleveland, Ohio, October 4, 1972,
501-04.

APPENDIX A

SYMBOLS

A	normalization constant
C	proportionality constant
c	speed of light, 3×10^{10} cm sec^{-1}
h	Planck constant, 6.626×10^{-34} joule sec^{-1}
I	intensity
j	rotational quantum number (initial state)
K	constant related to relative concentrations and cross sections of component gases
k	Boltzmann constant, 1.380×10^{-23} joule K^{-1}
R	half-width (FWHM), cm^{-1}
S	shape function
T	temperature, K
ΔT	standard deviation of temperature, K
θ	rotational characteristic temperature, K
ν	wavenumber, cm^{-1}
ν_0	wavenumber of incident light, cm^{-1}
$\Delta\nu$	wavenumber shift, cm^{-1}
ρ	molar concentration
σ	Raman-scattering cross section, $cm^3\ sr^{-1}$
τ	lifetime, sec

Subscripts:

F	filter
j	quantum number of initial state
L	laser
N	nitrogen gas
O	oxygen gas
P	pressure
R	Raman

s slit

Superscripts:

AS anti-Stokes

N nitrogen gas

O oxygen gas

S Stokes

APPENDIX B

APPARATUS AND EXPERIMENTAL TECHNIQUES

Test Apparatus

A laboratory Raman spectrophotometer was constructed to provide experimental data to compare with the theory. The instrument was used to make Raman spectrum measurements of gaseous dry air over a temperature range from 243 to 313 K at a pressure of 1 atmosphere. Basic units of the instrument are shown in the block diagram and accompanying photograph in figure 13.

The light source used for excitation was a continuous-wave argon-ion laser which was tunable to a number of discrete wavelengths through the use of an intracavity Littrow prism. For this investigation, it was operated at a wavelength of 488 nm (20 492 cm^{-1}), which provided approximately 200 milliwatts of multimode power. The output beam was linearly polarized to better than 1 part per 10^3 with the electric vector oriented vertically.

External optics (fig. 13) were employed to increase the scattered light radiance, as described in reference 17. After initially being directed toward the gas sample by a high-reflectivity mirror, the laser beam was passed through a crystalline half-wave plate which rotated the beam polarization by 90^o. (This was done to minimize the Rayleigh-scattered light being scattered toward the collecting optics.) The beam was condensed by a focusing lens to create a high-power-density scattering site in the gas sample. The optical path of the beam was terminated at a return mirror which refocused the beam back into the scattering site, thus creating repetitive passes of the beam through the gas sample and increasing scattered light radiance. The volume of maximum light scattering or the "Raman light source" could be approximated by a horizontal cylinder 20 micrometers in diameter and 2 millimeters in length (ref. 17). Included in the external optics was a light sensor which monitored the power of a secondary laser beam.

The gas samples were confined in a test cell approximately 10^{-3} cubic meter in volume. Temperature regulation of the gas was provided by flowing ethanol through the walls of the cell and using a controlled-temperature liquid bath. The temperature of both the cell and the gas was continuously monitored throughout each test. The optical windows in the cell through which the laser beam passed were parallel plates of coated quartz. At right angles to the axis of these windows were two optical ports which comprised a portion of the collecting optics system. At gas temperatures below the ambient dewpoint, all windows and ports were continuously purged with dry nitrogen to prevent fogging.

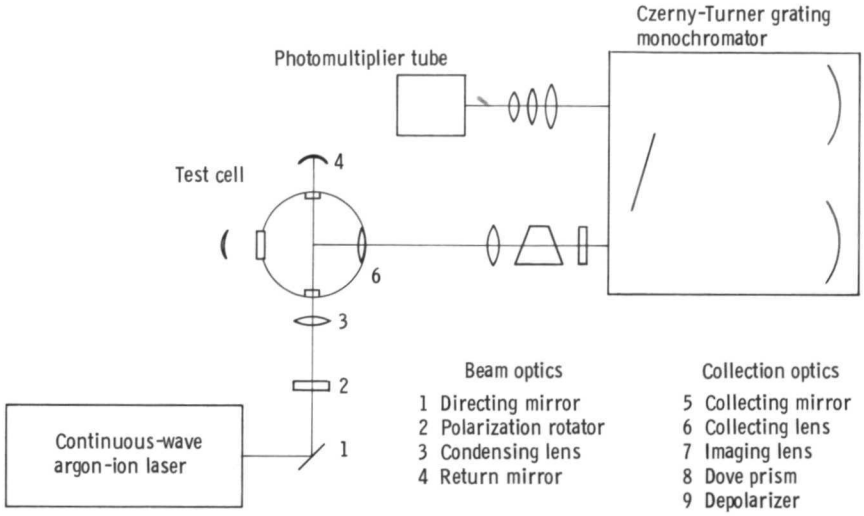

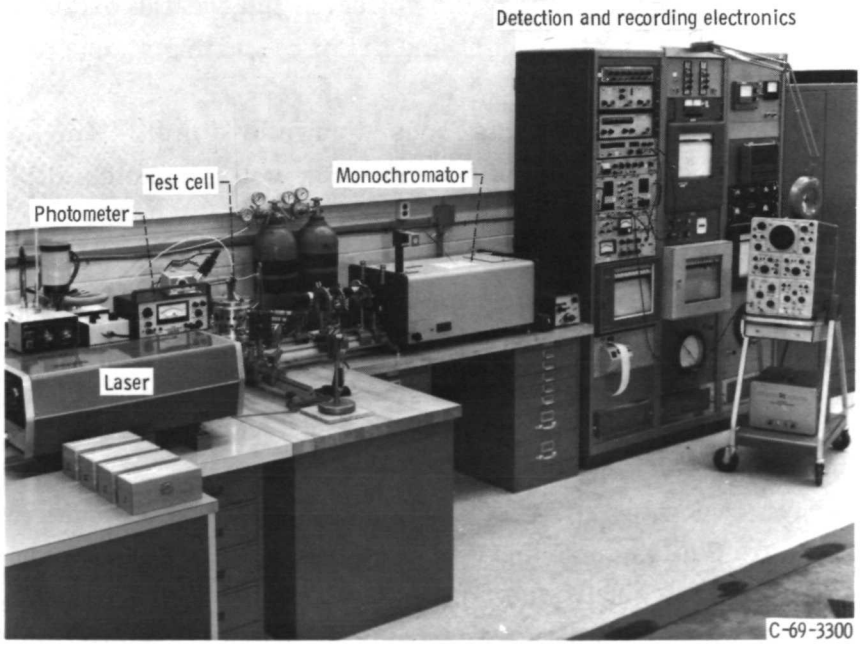

Figure 13. - Raman spectrophotometer.

Light scattered at right angles to the axis of the exciting laser beam was collected over a large solid angle by a lens which was a port in the cell. This lens, a field stop, and a secondary lens comprised an optical system (fig. 13) which magnified the image of the Raman source cylinder by a factor of 2.5 and matched the optical acceptance angle of the monochromator. By rotating the magnified image through 90^{o} with a dove prism, it was possible to efficiently fill the vertical entrance slit of the monochromator with collected light. The intensity of the collected light was enhanced by gathering that light which was scattered 180^{o} away from the primary collection lens with a concave mirror. A crystalline quartz wedge depolarized the light before incidence on the entrance slit.

Wavelength discrimination was provided by a single 3/4-meter Czerny-Turner grating monochromator. Both slits were operated at widths of 0.92, 1.84, and 2.76 cm^{-1} (mechanical slit widths of 20, 40, and 60 μm) which provided both efficient coupling with the collecting optics and adequate wavelength resolution. For this investigation, the wavelength scanning speed was set at 0.2 nm per minute ($\sim$8.4 cm^{-1}/min). Because the monochromator was only a single-pass instrument, stray light was a problem if the intensity of the collected Rayleigh light and spurious reflected laser light was very high. Fortunately, the Rayleigh-scattered light from oxygen and nitrogen was highly polarized, and its collected intensity was significantly reduced by the 90^{o} rotation of the exciting beam polarization. With this procedure, the collected light at the excitation wavelength was sufficiently reduced to keep stray light and primary grating ghosts at an insignificant level.

Light emerging from the exit slit was focused down by a multielement lens onto a 1-millimeter-diameter, S-20 surface of a Bendix channeltron photomultiplier tube. A highly stable power supply provided the multiplier bias (normally 2250 V). The small size of the photocathode surface and the low-noise characteristics of the multiplier circuit made it possible to operate the tube without cooling. When it was operated at room temperature, the combined noise and background count rate was about 20 counts per second.

The signal from the photomultiplier tube was sent through a system of photon counting (or pulse counting) electronics for amplification and display. Pulse signals were first passed directly to a low-noise preamplifier for impedance matching and first-stage amplification before transmission to the remaining rack-mounted electronics. A pulse-shaping linear amplifier then conditioned the signal for input into a pulse-height analyzer. The pulse-height analyzer served as a discriminator-trigger circuit so that each signal pulse was weighted equally and converted into a narrow-width pulse. The output from the pulse-height analyzer was directed to a digital recording system.

The digital recording system consisted of a 100-mHz scaler, a teletypewriter, and a paper-tape puncher. The scaler was gated to continuously count and record at 1-second intervals. Its output was recorded on paper tape by the interfacing electronics

and the teletypewriter. The data on the paper tape were then read and plotted by a high-speed computer. The result was a digital Raman rotational spectrum such as is shown in figure 1.

Experimental Procedure

Once the optical components were alined and the detecting electronics were conditioned for optimum pulse counting, the operation of the equipment was essentially routine, requiring only minor fine-tuning adjustments. Prior to each test, the electronic equipment and the laser were operated for a 30-minute warmup period. This was necessary for both stabilization of laser power and reduction of spurious counting noise. During this period, the gas cell was purged and filled with the desired gas and its temperature was adjusted.

With the system filled and stabilized, the optical components were adjusted for an optimum Raman signal. The rotational Raman spectra were then obtained by scanning from the oxygen anti-Stokes j=23 line at 484.7 nm (20 631 cm^{-1}) upward in wavelength through the oxygen Stokes j=23 line at 491.4 nm (20 350 cm^{-1}). All tests were conducted in the dark to reduce the background count rate. During the tests, all system variables were continuously monitored and recorded.

Because a direct comparison was to be made between the theoretical and experimental spectra, it was necessary to normalize the theoretical spectra to the correct maximum peak intensity.

The normalization was accomplished by referring to equations (II). It is shown in reference 6 that these equations accurately approximate the peak intensities of the nitrogen spectrum. Therefore, each experimental nitrogen line could be used to calculate a corresponding nitrogen j=6 peak intensity. Equations (I) could then be normalized such that the peak intensity of the j=6 line equaled the average of the intensities calculated by using equations (II).

To ensure accuracy, it was necessary to use only those lines that were either very nearly or completely resolved. These were determined by comparing nitrogen peak intensities obtained from a theoretical spectrum of air with those obtained from a line spectrum of nitrogen. Those that were the same or nearly the same were considered resolved.

Before making the direct comparison, it was also necessary to scale the experimental data for plotting purposes because the scan rate of the monochromator was not constant. Instead, it varied cyclically between 0.00357 to 0.00435 nm/sec (~0.150 to ~0.182 cm^{-1}/sec). Although small, this inconstancy caused a gross mispositioning of the spectral lines. To correct this difficulty, event markers were superimposed on the

spectra every 0.5 nm (~21 cm^{-1}) by the monochromator. Although of an insufficient frequency to correct for the variable scan rate, it did show that equations (VI) accurately located the nitrogen lines. The nitrogen lines, therefore, were used as scaling markers. By using equations (VI), the center of each even j-line was assigned its appropriate wavelength. The plotting routine used these positions to scale the experimental data accurately. The normalization and scaling procedures described here enabled the direct and accurate comparison of theoretical and experimental spectra.

REFERENCES

1. Melfi, Samuel H.: Raman Backscatter of Laser Radiation in the Earth's Atmosphere. Ph. D. Thesis, The College of William and Mary in Virginia, 1970.

2. Widhopf, George F.; and Lederman, Samuel: Specie Concentration Measurements Utilizing Raman Scattering of a Laser Beam. AIAA J., vol. 9, no. 2, Feb. 1971, pp. 309-316.

3. Kent, G. S.; and Wright, R. W. H.: A Review of Laser Radar Measurements of Atmospheric Properties. J. Atmos. Terrest. Phys., vol. 32, May 1970, pp. 917-943.

4. Cooney, John: Satellite Observations Using Raman Component of Laser Backscatter. Proceedings of the Symposium on Electromagnetic Sensing of the Earth from Satellites. Ralph Zirkind, ed., Polytechnic Institute of Brooklyn Press, 1967, pp. P1-P10.

5. Leser, Robert J.; and Salzman, Jack A.: Light-Detection Electronics for a Raman Lidar. NASA TN D-6879, 1972.

6. Salzman, Jack A.; Masica, William J.; and Coney, Thom A.: Determination of Gas Temperatures from Laser-Raman Scattering. NASA TN D-6336, 1971.

7. Garbuny, Max: Optical Physics. Academic Press., 1965.

8. Penner, S. S.: Quantitative Molecular Spectroscopy and Gas Emissivities. Adison-Wesley Publ. Co., Inc., 1959.

9. Dennison, David M.: The Shape and Intensities of Infra-Red Absorption Lines. Phys. Rev., vol. 31, no. 4, Apr. 1928, pp. 503-519.

10. Nielsen, J. Rud; Thornton, V.; and Dale, E. Brock: The Absorption Laws for Gases in the Infra-Red. Rev. Mod. Phys., vol. 16, no. 3-4, July-Oct. 1944, pp. 307-324.

11. Brodersen, Svend: Slit-Width Effects. J. Opt. Soc. Am., vol. 44, no. 1, Jan. 1954, pp. 22-25.

12. Stiocheff, B. P.: High Resolution Raman Spectroscopy. Advances in Spectroscopy. Vol. I. H. W. Thompson, ed., Interscience Publ., Inc., 1959.

13. Gray, Dwight E., ed.: American Institute of Physics Handbook. Second ed., McGraw-Hill Book Co., Inc., 1963.

14. Pinter, F.: Dependence of the Width of the Rotational Raman Lines of N_2 and CO_2 on the Quantum Number j. Optics Spectrosc., vol. 17, no. 5, Nov. 1964, pp. 428-429.

15. Lazarev, Yu. A : Line Broadening in Rotational and Rotation-Vibrational Raman Spectra of Gases. Optics Spectrosc., vol. 13, no. 5, Nov. 1962, pp. 373-376.

16. Weast, Robert C., ed.: Handbook of Chemistry and Physics. 47th ed., Chemical Rubber Co., 1966.

17. Barrett, J. J.; and Adams, N. I., III: Laser - Excited Rotation - Vibration Raman Scattering in Ultra-Small Gas Samples. J. Opt. Soc. Am., vol. 58, no. 3, Mar. 1968, pp. 311-319.

NASA-Langley, 1973 —— 16 E-7045

1. Report No.	2. Government Accession No.	3. Recipient's Catalog No.
NASA TN D-7126		

4. Title and Subtitle	5. Report Date
DETERMINATION OF THE TEMPERATURE OF GAS MIXTURES BY USING LASER RAMAN SCATTERING	January 1973
	6. Performing Organization Code

7. Author(s)	8. Performing Organization Report No.
Thom A. Coney and Jack A. Salzman	E-7045
	10. Work Unit No.
	501-04

9. Performing Organization Name and Address	11. Contract or Grant No.
Lewis Research Center National Aeronautics and Space Administration Cleveland, Ohio 44135	
	13. Type of Report and Period Covered
12. Sponsoring Agency Name and Address	Technical Note
National Aeronautics and Space Administration Washington, D.C. 20546	14. Sponsoring Agency Code

15. Supplementary Notes

16. Abstract

A theoretical model for the Raman rotational spectrum of air was formulated, yielding the spectral temperature dependence; and an error analysis of temperature measurement accuracies was performed. The theoretical spectra and the predicted temperature measurement error of ±20 K (~7 percent) compared well with experimental data. These experimental data consisted of Raman spectra of air obtained for temperatures ranging from 243 to 313 K at a pressure of 1 atmosphere. The use of selected lines resulted in an experimental accuracy of ±13 K (~5 percent).

17. Key Words (Suggested by Author(s))

Temperature
Raman scattering
Air
Laser
Lidar

18. Distribution Statement

Unclassified - unlimited

19. Security Classif. (of this report)	20. Security Classif. (of this page)	21. No. of Pages	22. Price*
Unclassified	Unclassified	35	$3.00

* For sale by the National Technical Information Service, Springfield, Virginia 22151

"The aeronautical and space activities of the United States shall be conducted so as to contribute . . . to the expansion of human knowledge of phenomena in the atmosphere and space. The Administration shall provide for the widest practicable and appropriate dissemination of information concerning its activities and the results thereof."

—NATIONAL AERONAUTICS AND SPACE ACT OF 1958

NASA SCIENTIFIC AND TECHNICAL PUBLICATIONS

TECHNICAL REPORTS: Scientific and technical information considered important, complete, and a lasting contribution to existing knowledge.

TECHNICAL NOTES: Information less broad in scope but nevertheless of importance as a contribution to existing knowledge.

TECHNICAL MEMORANDUMS: Information receiving limited distribution because of preliminary data, security classification, or other reasons. Also includes conference proceedings with either limited or unlimited distribution.

CONTRACTOR REPORTS: Scientific and technical information generated under a NASA contract or grant and considered an important contribution to existing knowledge.

TECHNICAL TRANSLATIONS: Information published in a foreign language considered to merit NASA distribution in English.

SPECIAL PUBLICATIONS: Information derived from or of value to NASA activities. Publications include final reports of major projects, monographs, data compilations, handbooks, sourcebooks, and special bibliographies.

TECHNOLOGY UTILIZATION PUBLICATIONS: Information on technology used by NASA that may be of particular interest in commercial and other non-aerospace applications. Publications include Tech Briefs, Technology Utilization Reports and Technology Surveys.

Details on the availability of these publications may be obtained from:

SCIENTIFIC AND TECHNICAL INFORMATION OFFICE

NATIONAL AERONAUTICS AND SPACE ADMINISTRATION

Washington, D.C. 20546